TÜBİTAK

Turk J Phys
33 (2009) , 101 – 108.

doi:10.3906/fiz-0810-15

Generation of Ultrafast Bright and Dark Pulse on Silicon Chip with Integrated Mach-Zehnder Interferometer Configuration

Jianwei WU[1], **Fengguang LUO**[2,3]
[1] *Institute of Optoelectronics Science & College of Mathematics and Physics, Hohai University, Nanjing 210098, P. R. CHINA*
e-mail: jwwu@hhu.edu.cn
[2] *Wuhan National Laboratory for Optoelectronics, Wuhan 430074, P. R. CHINA*
[3] *College of Optoelectronics Science and Engineering, Huazhong University of Science and Technology, Wuhan 430074, P. R. CHINA*

Received 14.10.2008

Abstract

In this paper we propose and simulate ultrafast femtosecond bright and dark pulses, obtained simultaneously at the same center wavelength, based on silicon-on-insulator (SOI) waveguides in Mach-Zehnder interferometer (MZI) configuration; the ultrafast pulsed pump is injected into one MZI's arm and a continuous wave component (CW) is divided equally into the two MZI arms. Numerical results show that properties of the generated bright and dark pulses are strongly dependent on the launching optical powers of both the pump pulse and CW carriers, and on the waveguide length.

Key Words: Integrated optics, silicon-on-insulator technology, ultrafast process, pulse generation.

1. Introduction

Ultrafast pulse sources are very important for applications in diverse fields such as optoelectronics and spectroscopy. Many schemes have been explored so far, in which the generation of broadband, tunable ultrafast bright pulses is very attractive when based on the effect of Stimulated Raman Scattering (SRS) [1, 2]. On the other hand, ultrafast dark pulses have attracted considerable attention due to their advantages in loss, noise, and mutual interactions between adjacent pulses compared with their bright counterparts. Numerous projects have obtained significant dark pulses, but under complex experimental setups. The literature describing these results often cite approaches involving cross-phase modulation in optical fibers and modulation instability [3, 4]. Such approaches require long fiber lengths to produce the effective nonlinear process, among other elements

combined, to attain pulse compression/reshaping. These requirements are hard to implement in integrated optics for the low-cost market. In such schemes the obtained dark pulse has very low-contrast ($\sim$23%) and increased pedestal when further propagated in fibers, with the pulse width of tens of picoseconds, restricting further advances in high-speed signal processing. The above mentioned references use separate devices for the generation of bright and the dark pulses.

Motivated by these limitations, we suggest here the use of silicon-on-insulator (SOI) to produce the nonlinear interaction, which is promising for optoelectronics integration and ultrafast signal generation in the femtosecond range.

Due to improvement in the last few years of material integration techniques, silicon photonics has attracted attention since there are many possibilities to implement passive and active devices with new or improved functionalities [5]. One such approach for new devices is based on SOI waveguides with sub-micrometer transverse dimensions. Such SOI devices can present strong light confinement and lead to enhanced nonlinear effects, mainly due to the high refractive index ratio between the silicon core and the silica cladding. So, strong nonlinear effects can occur in millimeter- or centimeter-long silicon waveguides. In general, two possible SOI waveguide structures are adopted for applications, namely the strip and the ridge waveguides. To achieve single mode operation a strip waveguide must be small in dimensions, and this creates challenges in optical coupling and electrical access procedures. On the other hand, ridge waveguides can be larger in size and even work in single-mode operation, and thus usually is the preferred choice in practical applications [6].

Therefore, the SOI ridge waveguides were adopted for our following investigations. By utilizing the physical properties of SOI waveguide, an integrated Mach-Zehnder interferometer (MZI) configuration device has been designed in order to achieve simultaneous generation of ultrafast bright and dark pulses, with pulse widths of femtosecond duration at the same wavelength.

2. Modeling and Equations

The designed MZI configuration setup and cross-section of SOI ridge waveguide are illustrated in Figure 1(a) and (b), respectively. In Figure 1(a), two identical SOI waveguides are used in MZI configuration, Y1 and Y2 are the 3 dB Y-couplers, C1 and C2 are the 3 dB directional couplers, and F1 and F2 are the filters which will cutoff the pump pulse. The working principle for the pulse generation can be described as follows: the continuous wave (CW) channel is equally divided into the upper- and lower-arm of MZI by C1, and then in the upper-arm the CW-channel is combined with the pulsed pump channel before being coupled into the SOI, where the pulsed pump will act by means of nonlinear process resulting in the additional phase change into the CW-channel; in the lower-arm the CW-channel directly pass through the SOI. As consequence the phase difference between the divided CW-channels will produce ultrafast bright and dark pulses at the MZI output due wave-interference effects. In Figure 1(b) is shown a ridge waveguide structure with width W, rib height H, and slab height h. Free electrical carriers are produced when light is absorbed inside lower the SOI waveguide, whose effective recombination lifetime τ_{eff} may be denoted by [7]

$$\tau_{\text{eff}}^{-1} = \frac{S}{H} + \frac{w + 2(H-h)}{wH} S' + 2\frac{h}{H}\sqrt{\frac{D}{w^2}\left(\frac{S+S'}{h}\right)} \tag{1}$$

where the first term refers to the interface's recombination lifetime, the second term to the surface recombination at the sidewalls, and the last term to the transit time out of the modal area. S and S' are the effective surface recombination velocities, D is diffusion coefficient.

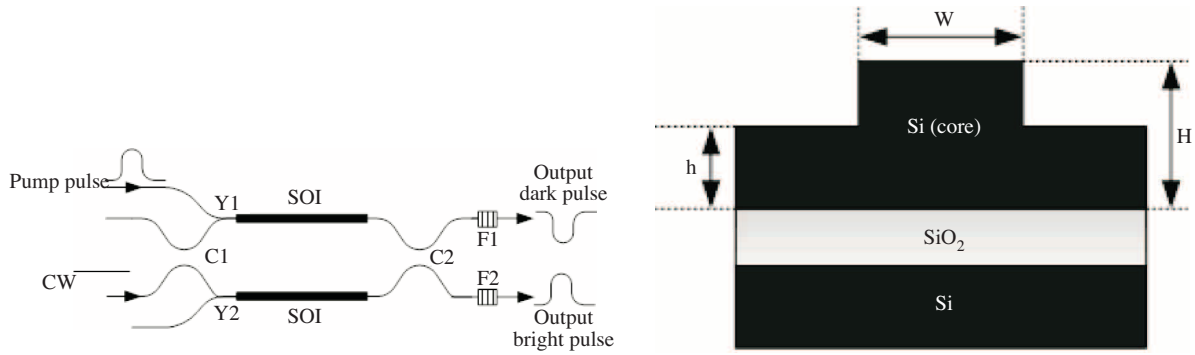

Figure 1. (a). The schematic diagram of MZI configuration. (b). The cross-section of SOI ridge waveguide.

The nonlinear propagation equations for the CW and the pump pulse channels in the SOI waveguide for the MZI's upper-arm can be described by [8, 9]:

$$\begin{aligned}&\tfrac{\partial A_c}{\partial z}+\beta_{c1}\tfrac{\partial A_c}{\partial t}+i\tfrac{1}{2}\beta_{c2}\tfrac{\partial^2 A_c}{\partial t^2}-\tfrac{1}{6}\beta_{c3}\tfrac{\partial^3 A_c}{\partial t^3}=\\&\quad-\tfrac{1}{2}\alpha_{cl}A_c-\tfrac{1}{2}\alpha_{cFC}A_c-\tfrac{1}{2}\tfrac{\beta_{ccTPA}}{A_{cAeff}}\left|A_c\right|^2A_c-\tfrac{\beta_{cdTPA}}{A_{cAeff}}\left|A_d\right|^2A_c\\&\quad+i\gamma_{c,c}\left|A_c\right|^2A_c+i2\gamma_{c,d}\left|A_d\right|^2A_c+i\tfrac{2\pi}{\lambda_c}\Delta n_{\lambda_c}A_c\end{aligned}\tag{2}$$

$$\begin{aligned}&\tfrac{\partial A_d}{\partial z}+\beta_{d1}\tfrac{\partial A_d}{\partial t}+i\tfrac{1}{2}\beta_{d2}\tfrac{\partial^2 A_d}{\partial t^2}-\tfrac{1}{6}\beta_{d3}\tfrac{\partial^3 A_d}{\partial t^3}=\\&\quad-\tfrac{1}{2}\alpha_{dl}A_d-\tfrac{1}{2}\alpha_{dFC}A_d-\tfrac{1}{2}\tfrac{\beta_{ddTPA}}{A_{dAeff}}\left|A_d\right|^2A_d-\tfrac{\beta_{dcTPA}}{A_{dAeff}}\left|A_c\right|^2A_d\\&\quad+i\gamma_{d,d}\left|A_d\right|^2A_d+i2\gamma_{d,c}\left|A_c\right|^2A_d+i\tfrac{2\pi}{\lambda_d}\Delta n_{\lambda d}A_d\end{aligned}\tag{3}$$

The propagation equation of CW in SOI waveguide of the lower-arm is described by the equation

$$\begin{aligned}\tfrac{\partial A_d}{\partial z}+\beta_{d1}\tfrac{\partial A_d}{\partial t}=&-\tfrac{1}{2}\alpha_{dl}A_d-\tfrac{1}{2}\alpha_{dFC}A_d\\&-\tfrac{1}{2}\tfrac{\beta_{ddTPA}}{A_{dAeff}}\left|A_d\right|^2A_d+i\gamma_{d,d}\left|A_d\right|^2A_d+i\tfrac{2\pi}{\lambda_d}\Delta n_{\lambda d}A_d,\end{aligned}\tag{4}$$

where the subscripts c and d denote pump pulse and the CW channel, respectively. A is the slowly-varying pulse envelop, β_1, β_2 and β_3 are the first-, second- and third-order dispersion coefficients. Parameter β_1 is related to the group velocity by $\nu_g=1/\beta_1$, while β_2 governs the effect of Group Velocity Dispersion (GVD), β_3 governs the effects of Third Order Dispersion (TOD) and so are important for the application of ultrashort pulses due the needed wide bandwidth. The factor $\gamma=2\pi n_2/\lambda A_{Aeff}$ is the nonlinear parameter (n_2 is the nonlinear coefficient, and A_{Aeff} is known as the effective core area, λ is the center wavelength of optical wave.), α_l is the linear propagation loss. α_{FC} is the Free Carrier Absorption (FCA) coefficient, β_{TPA} is the Two-Photon Absoption (TPA) coefficient, which has identical values for all kinds of TPA processes, and ω is

the angle frequency. The first four terms on the right-hand side of each equation denote the propagation loss, FCA loss, degenerate TPA and non-degenerate TPA, respectively. The next two terms represent the self-phase modulation (SPM) and cross-phase modulation (XPM), respectively, and the final term describes free carrier dispersion (FCD) that is related to efficient index change Δn, as described in [10]:

$$\Delta n_{\lambda c,d} = -8.8 \times 10^{-22} \cdot (\frac{\lambda_{c,d}}{1.55})^2 \Delta n_e - 8.5 \times 10^{-18} \cdot (\frac{\lambda_{c,d}}{1.55})^2 (\Delta n_h)^{0.8} \tag{5}$$

and the FCA coefficient is written as

$$\begin{aligned} \alpha_{FC} &= 8.5 \times 10^{-18} \cdot (\tfrac{\lambda_{c,d}}{1.55})^2 \Delta n_e + 6.0 \times 10^{-18} \cdot (\tfrac{\lambda_{c,d}}{1.55})^2 \Delta n_h \\ &= \sigma \cdot n \\ &= \sigma_0 \cdot (\tfrac{\lambda_{c,d}}{1.55})^2 n, \end{aligned} \tag{6}$$

where σ_0=1.45×10^{-17} cm^2 is the free-carrier absorption cross section measured at λ=1.55 μm. $n = n_e = n_h$ is the density of electron-hole pairs generated by the TPA and non-degenerated TPA processes, and given by [11]:

$$\begin{aligned} \tfrac{dn}{dT} = &-\tfrac{n}{\tau_{\text{eff}}} + \tfrac{\beta_{ccTPA}}{2\hbar\omega_c}(|A_c(z,t)|^2 \cdot A_{cAeff}^{-1})^2 + \tfrac{\beta_{ddTPA}}{2\hbar\omega_d}(|A_d(z,t)|^2 \cdot A_{dAeff}^{-1})^2 \\ &+ \tfrac{\beta_{cdTPA}}{\hbar\omega_d}(|A_d(z,t)|^2 \cdot A_{cAeff}^{-1})^{\ 2} + \tfrac{\beta_{dcTPA}}{\hbar\omega_c}(|A_c(z,t)|^2 \cdot A_{dAeff}^{-1})^2 \end{aligned} \tag{7}$$

To observe the characteristics of the ultrafast bright and dark pulse generation, equations (1)-(7) can be solved numerically for determined boundary conditions. In the following sections, the detailed numerical investigations are presented.

3. Numerical Simulations and Discussion

Keeping in mind the literature [7, 12], we adopt model parameters as shown in Table 1. In these simulations, the input pump pulses are assumed to be Gaussian in shape as $A_c(0, T)=(P_{c0})^{1/2}\exp[-1/2\cdot(T/T_{c0})^2]$, and the CW-channel is expressed as $A_d(0, T)=(P_{d0})^{1/2}$, in which the T_{c0} is half width at 1/e intensity point, and P_{c0}, and P_{d0} are respectively the initial pump and the CW optical powers. The influence of the pump power on the generated pulse is shown in Figure 2, where Figure 2(a) and (b) plot respectively the bright and dark pulses generated for three pump powers - P_{c0} = 1 W, 3 W, and 5 W and Figure 2(c) displays the corresponding phase difference for the CW optical fields between the two MZI arms at the output, using T_{c0}=100 fs, P_{d0}=0.1 W, and SOI length, L=5 mm. As can be seen from the Figure 2, the pedestal of the bright pulse is enhanced as increased the pump power, which will produce inter-channel interference for the adjacent pulses and can lead to system's decay in performance. Such behave can be explained by that, because the pump power is very strong comparing with the CW power, the free-carrier density induced by TPA process are dominant in the silicon-MIZ upper-arm, so that the phase of CW-channel behind the pump pulse will be changed due to the free-carrier effect, leading to remarkable phase difference for the CW between upper- and lower-arm, which can be seen in Figure 2(c) where the phase difference for generating bright pulse is not equal to π, resulting in the pedestal, which is shown in Figure 2(a), where the lasting time of pedestal will be as long as hundreds of picoseconds, mainly due to long free-carrier's recovery time. Another issue is that the contrast of the dark pulses is linearly

increased with the pump power, since the pump pulse will act on the CW-channel by nonlinear processes such as XPM, TPA and FCD. Furthermore, the nonlinear processes will become stronger with increased pump power, resulting in larger phase difference between both of upper- and lower-arm that is shown in Figure 2(c). where the phase difference for generating dark pulse is not equal to zero in the region of dark pulse. Therefore, it is very obvious that the contrast of dark pulse takes on the trend enhanced with increase of pump power, e.g. the contrast is about 10% at $P_{c0} = 1$ W because of small phase difference induced by low level pump power, and will be increased to about 35% at $P_{c0} = 3$ W, and will be further arrive at about 55% at $P_{c0} = 5$ W, owing to large phase change in the upper-arm for high pump power level. In addition, it is noticeable that the free pedestal is at the leading edge of generated pulse because the CW part before the pump will not be influenced by the pump pulse so that their phase difference is always equal to π resulting in the completely destructive interference. Based on above analysis, we can not balance the behaviors of decreasing the pedestal and enhancing the contrast by means of increasing the initial pump power. Motivated by the phenomena, researches were done to see the influence of the input CW optical power on the output pulse, as shown next.

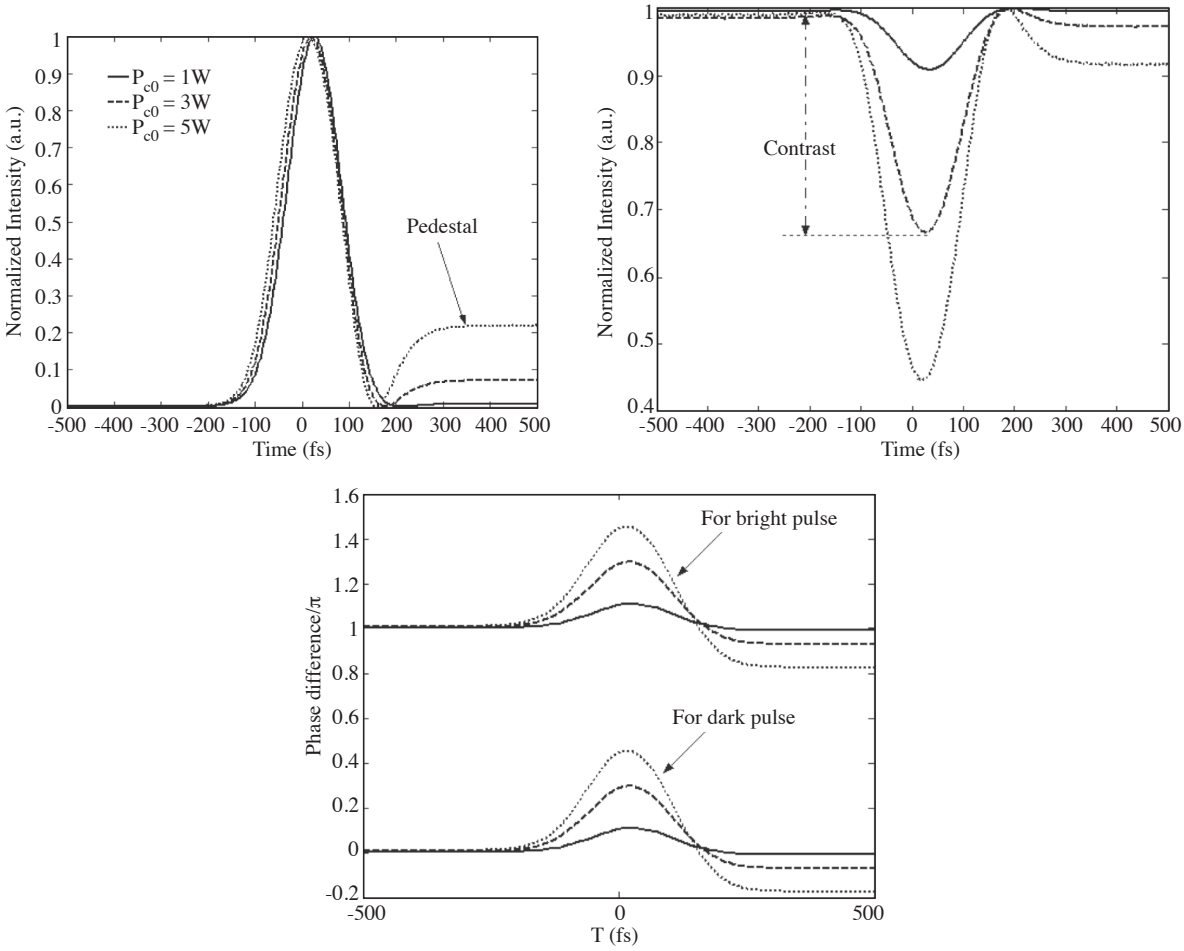

Figure 2. The profiles of generated bright (a), dark (b) pulses and phase difference (c) with different initial pump power.

Table 1. The adopted system parameters in numerical simulation.

Parameter	Definition	Value
λ_c	Pump wavelength	1550 nm
λ_d	CW wavelength	1480 nm
n_2	Nonlinear coefficient	6×10^{-18} m^2·W^{-1}
β_{c1}	The first-order dispersion at pump wavelength	1.351×10^{-8} s·m^{-1}
β_{c2}	The second-order dispersion at pump wavelength	0
β_{c3}	The third-order dispersion at pump wavelength	4.1×10^{-3} ps^3·m^{-1}
β_{d1}	The first-order dispersion at CW wavelength	1.353×10^{-8} s·m^{-1}
β_{d2}	The second-order dispersion at CW wavelength	0.3 ps^2·m^{-1}
β_{d3}	The third-order dispersion at CW wavelength	3.8×10^{-3}ps^3·m^{-1}
$\alpha_{cl,dl}$	Waveguide linear loss coefficient	0.22 dB·cm^{-1}
β_{TPA}	Two-photon absorption coefficient	0.5 cm/GW^{-1}
W	Rib waveguide width	900 nm
H	Rib height	780 nm
H	Slab height	390 nm
$S, S^{'}$	Effective surface recombination velocity	80 m·s^{-1}
D	Diffusion coefficient	16 cm·s^{-1}
H	Reduced Planck constant	1.06×10^{-34} J·s

Figure 3(a) and (b) display, respectively, the generated bright and dark pulses for different input CW optical power–P_{d0} = 1, 5 and 10 W—when the input pump optical power is set to P_{c0} = 5 W, and the other simulation parameters are same as before (Iigure 2.). From the Figure 3 it is clearly shown that the pedestal of the bright pulse will decay gradually with the CW input power increasing, however the contrast of the dark pulses are gently changed in these cases. The phenomena can be explained by that, when the CW channel power is lower than the pump power, the free-carriers induced by the pump pulse are dominant, resulting in a pedestal at the trailing edge of output bright pulses. But when the CW power is increased the free carriers induced by CW-channel will dominate the nonlinear refractive index change in the silicon waveguide, leading to

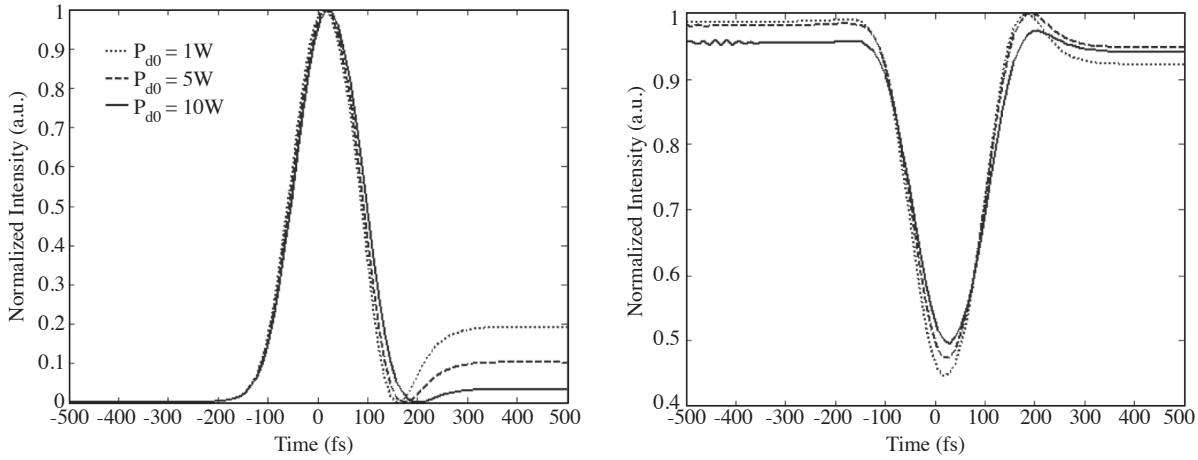

Figure 3. The profiles of generated bright (a) and dark (b) pulses with different initial CW power.

the pedestal of bright pulse suppressed, which can be seen in the case of $P_{d0} = 10$ W. On the other hand, when the CW power varies from 1 W to 10 W, the contrast of dark pulse is changed slightly, and maintains always the level of about 50%. The phenomenon impact on the quality of generated dark pulses, and depends mainly on the properties of the pump pulse. Therefore, we should increase the CW power to improve the quality of bright pulse. In case of changing the pump or the CW power, the obtained bright and dark pulses have nearly the same width as the initial pump pulse due to the short waveguide length, which reduce the influences of dispersion and group velocity mismatch between the pump and the CW optical fields. In fact, if we extend the waveguide length the dispersion and group velocity mismatch will play important roles in changing the pulse generation performance, as discussed next.

Figure 4(a) and (b) show respectively the waveforms of bright and dark pulses with $P_{c0} = 2$W and $P_{d0} = 0.1$W, for a waveguide lengths L of 5 mm, 10 mm, and 15 mm. As can be seen at Figure 4(a), the pedestal of the bright pulse is very low due to the low input pump optical power. In addition, the pulse width and contrast for the dark pulses are enhanced rapidly with the waveguide length, as displayed in Figure 4(b), in which the origins of phenomenon are that the influences of dispersion and group velocity mismatch are enhanced significantly due to the increase of waveguide length, i.e., by the means of extending the waveguide the nonlinear interaction length can be extended leading to large phase difference between both arms, and as a result the contrast of dark pulses is improved rapidly, up to 50% at $L = 15$ mm. In addition, the group velocity mismatch will produce remarkable effect on the propagating optical fields, resulting in the spread of the overlapped range between the pump pulse and the CW channels, and as a consequence the width of the generated pulse is extended, comparing to the case of a shorter waveguide. In fact, to reduce the influence of the GVD in the wave propagation the GVD parameter for the pump wavelength has been fixed as zero so that the dispersion will produce slight influence on the quality of the output pulse.

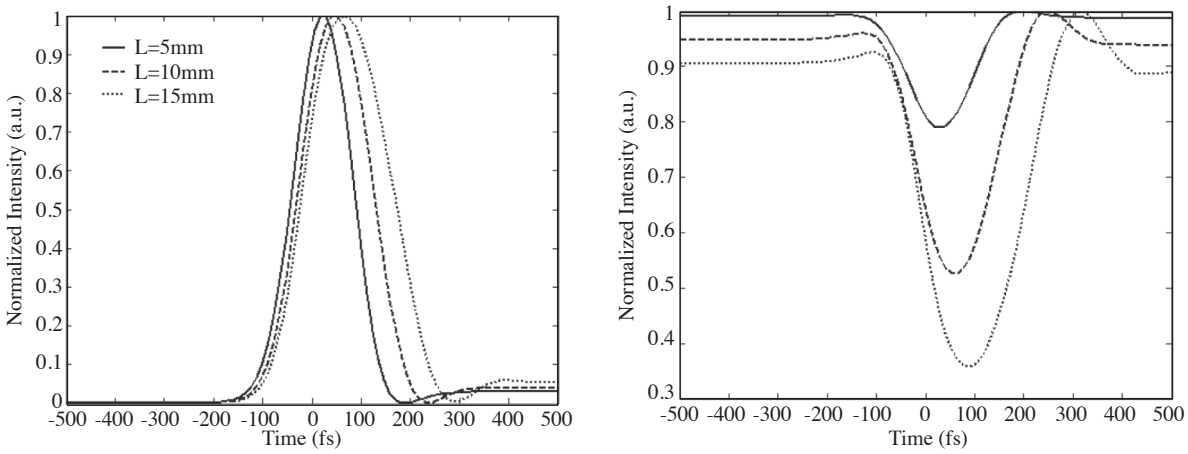

Figure 4. The profiles of generated bright (a) and dark (b) pulses with different waveguide length.

4. Conclusions

The numerical demonstration of an integrated MZI configuration with SOI optical waveguides to simultaneously generate bright and dark pulses has been presented. The basic operation principle is the phase-crosstalk induced by an ultrafast pump pulse channel to a CW optical field, converted to amplitude cross-modulation

by the MZI device in such a way that bright and dark pulses appear at the two output ports. The quality of the output pulses depends strongly on the optical power levels of both pump and CW channels and on the waveguide length. To generate high quality output pulse the CW and pump pulse powers should be adjust initially, and the silicon waveguide length optimized after.

Acknowledgements

This work was supported by the Chinese Natural Science Foundation under grant #60677023, the Chinese National High technology Research and Development Program under grant #2006AA01Z240.

References

[1] D. B. S. Soh, J. Nilsson and A. B. Grudinin, *J. Opt. Soc. Am. B-Opt. Phys.*, **23**, (2006),1.

[2] K. Wu, J. Wu and H. P. Zeng, *J. Phys. B- Ato. Mol. Opt.*, **36**, (2003), L349.

[3] W. H. Cao, S. P. Li and K.T. Chan, *Appl. Phys. Lett.*, **74**, (1999), 510.

[4] T. Svlvestre, S. Coen, P. Emplit and M. Haelterman, *Opt. Lett.*, **27**, (2002), 482.

[5] B. Jalali and S. Fathpour, *J. Lightwave Technol.*, **24,** (2006), 4600.

[6] W. N. Ye, PhD thesis, Department of Electronics, Carleton University, Canada, 2006.

[7] D. Dimitropoulos, J. R. Claps, J.C.S. Woo and B. Jalali, *Appl. Phys. Lett.*, **86**, (2005), 07115.

[8] V. M. N. Passaro and F. De Leonardis, *Opt. and Quantum Electron.*, **38**, (2006), 877.

[9] V. M. N. Passaro and F. De Leonardis, *J. Lightwave Technol.*, **24**, (2006), 2920.

[10] R. A. Soref and B. R. Bennett, *IEEE. J. Quantum Electron.*, **QE-23**, (1987), 123.

[11] A. S. Liu, H. S. Rong, M. Paniccia, O. Cohen and D. Hak, *Opt. Express*, **12**, (2004), 4261.

[12] Q. Lin, J.D. Zhang, P. M. Fauchet and G.P. Agrawal, *Opt. Express*, **14**, (2006), 4786.